AIAA-97-2573

NUMERICAL STUDY OF HYPERSONIC VISCOUS FLOW ABOUT PLATES LOCATED BEHIND A CYLINDER

I. V. Yegorov,* M. V. Yegorova,† and D. V. Ivanov‡
Central Aero-Hydrodynamics Institute
Zhukovsky-3, Moscow region, Russia 140160
and
V. V. Riabov§
Worcester Polytechnic Institute
Worcester, Massachusetts 01609-2280, USA

Abstract

A new implicit monotonized scheme of second-order accuracy and Newton's method for solving the grid equations approximated the Navier-Stokes equations were developed to simulate the two-dimensional hypersonic viscous flow about a plate located in the wakes of a cylinder. The strong influence of the geometrical factor of interference between a plate and a cylinder (characterized by the normalized distance between the bodies) on skin friction and heat flux along the plane and cylinder surfaces have been found. The changes of temperature, pressure and velocity fields in the wake behind the cylinder have been analyzed.

Nomenclature

C_f = local skin friction coefficient
c_p = specific heat at constant pressure
c_v = specific heat at constant volume
$\mathbf{E}$ = flux-vector in curvilinear coordinate system, Eqs. (1), (2)
e = total energy per unit volume, $\rho(c_vT+(u^2 + v^2)/2)$
$\mathbf{G}$ = flux-vector in curvilinear coordinate system, Eqs. (1), (2)
H = total enthalpy per unit volume, $c_pT + (u^2 + v^2)/2$
h = node size
J = Jacobian of the coordinates transformation
k = Boltzmann's constant
L = length of the plate
m = molecular mass
Pr = Prandtl number
p = pressure
$\mathbf{Q}$ = vector of dependent variables, Eq. (1)
$\mathbf{q}$ = heat flux vector
Re = Reynolds number, $\rho_\infty u_\infty r/\mu_\infty$
r = radius of the cylinder
T = temperature
u = x-velocity component
$\mathbf{V}$ = velocity vector
v = y-velocity component
x = Cartesian x-coordinate
y = Cartesian y-coordinate
γ = specific heat ratio, c_p/c_v
Δ = distance between the plate leading edge and the cylinder rear point
η = curvilinear coordinate
λ = conductivity coefficient
λ_i = eigenvalue
μ = viscosity coefficient
ξ = curvilinear coordinate
ρ = density of fluid
τ_k = regularization parameter, Eq. (15)
τ_{xy} = viscous stress tensor
ϕ = function, Eq. (9)
ε = small parameter, Eq. (9)

Subscripts

c = Cartesian coordinate system
w = wall value
∞ = freestream value

*Leading Scientist, Aerothermodynamics Division.
†Research Scientist, Aerothermodynamics Division.
‡Junior Research Scientist, Aerothermodynamics Division.
§Adjunct Associate Professor, Department of Mechanical Engineering, 100 Institute Road. Member AIAA.

Introduction

The structures of hypersonic viscous flow near a sharp flat plate and a cylinder were studied in detail by many researches (i.e., see Refs. 1-6). Hayes and Probstein[1], Oguchi[2], Allegre and Bisch[3], and others showed that the local skin friction coefficient, the surface pressure, and temperature are maximal near the leading edge of the plate. In a strong interaction hypersonic-flow regime, the influence of the skin friction drag on the total drag can be estimated as 80-90%.[7] Bisch[7] offered a unique experimental technique of the friction reduction by adding a wire-shaped "fore-leading edge" in front of the plate. The experiments of Coudeville et al[5] were helpful for the analysis of the wakes behind cylinders in hypersonic rarefied gas flow.

In the present analysis, the major regularities in hypersonic viscous flow about a plate located in the wakes of a circular cylinder have been studied. The analysis of two-dimensional flow structure is based on numerical solutions of the Navier-Stokes equations using a new implicit monotonized scheme of second-order accuracy (TVD-scheme) and Newton's method for solving the grid equations. The influence of the geometrical factors of interference between a plate and a cylinder (i.e., the distance between the leading edge of a plate and a rear point of a cylinder, Δ) on skin-friction, heat flux, and pressure and temperature distributions in the flow field and along the surfaces of the bodies has been studied.

Navier-Stokes Equations and Boundary Conditions.

The unsteady two-dimensional Navier-Stokes equations in a curvilinear coordinate system (ξ,η), $x = x(\xi,\eta)$, $y = y(\xi,\eta)$, where x, y are Cartesian coordinates have a conservation form:[8]

$$\frac{\partial \mathbf{Q}}{\partial t}+\frac{\partial \mathbf{E}}{\partial \xi}+\frac{\partial \mathbf{G}}{\partial \eta}=0 \qquad (1)$$

Here $\mathbf{Q}$ is a dependent-variables vector, $\mathbf{E}$ and $\mathbf{G}$ are flux-vectors in curvilinear coordinate system. $\mathbf{Q}$, $\mathbf{E}$ and $\mathbf{G}$ vectors are corresponding to Cartesian vectors $\mathbf{Q}_c$, $\mathbf{E}_c$, and $\mathbf{G}_c$ as follow:

$$\begin{aligned}\mathbf{Q}&=\mathrm{J}\mathbf{Q}_c\\ \mathbf{E}&=\mathrm{J}\left(\mathbf{E}_c\frac{\partial \xi}{\partial x}+\mathbf{G}_c\frac{\partial \xi}{\partial y}\right)\\ \mathbf{G}&=\mathrm{J}\left(\mathbf{E}_c\frac{\partial \eta}{\partial x}+\mathbf{G}_c\frac{\partial \eta}{\partial y}\right)\end{aligned} \qquad (2)$$

where $\mathrm{J} = \partial(x,y)/\partial(\xi,\eta)$ is a Jacobian of the coordinates' transformation.

The Cartesian vector components $\mathbf{Q}_c$, $\mathbf{E}_c$, and $\mathbf{G}_c$ for the two-dimensional Navier-Stokes equations have the following form:

$$\mathbf{Q}_c=\begin{Vmatrix}\rho\\ \rho u\\ \rho v\\ e\end{Vmatrix}$$

$$\mathbf{E}_c=\begin{Vmatrix}\rho u\\ \rho u^2+p-\tau_{xx}\\ \rho uv-\tau_{xy}\\ \rho uH-q_x\end{Vmatrix} \qquad (3)$$

$$\mathbf{G}_c=\begin{Vmatrix}\rho v\\ \rho uv-\tau_{xy}\\ \rho v^2+p-\tau_{yy}\\ \rho vH-q_y\end{Vmatrix}$$

The viscous stress tensor τ has the components:

$$\begin{aligned}\tau_{xx}&=\mu\left(-\frac{2}{3}\mathrm{div}\,\mathbf{V}+2\frac{\partial u}{\partial x}\right)\\ \tau_{xy}=\tau_{yx}&=\mu\left(\frac{\partial u}{\partial y}+\frac{\partial v}{\partial x}\right)\\ \tau_{yy}&=\mu\left(-\frac{2}{3}\mathrm{div}\,\mathbf{V}+2\frac{\partial v}{\partial y}\right)\end{aligned} \qquad (4)$$

The heat flux vector $\mathbf{q}$ is calculated by formula:

$$\mathbf{q}=\lambda\,\mathrm{grad}(T)+\tau\mathbf{V} \qquad (5)$$

The Navier-Stokes equation system (1) for compressible perfect gas model is completed by the state equation:

$$p = \rho k T/m \qquad (6)$$

Also, it is assumed that the coefficient of viscosity is calculated by the power low of the variation of this coefficient with temperature, $\mu/\mu_\infty = (T/T_\infty)^{0.7}$, and the Prandtl number is constant, $Pr = 0.7$.

For further numerical analysis, new non-dimensional parameters in Eqs. (1) - (6) were set up by normalizing the Cartesian coordinates to the characteristic length scale r (the radius of a cylinder), the Cartesian velocity components - to the upstream velocity u_∞, the pressure - to the double value of the dynamic pressure in upstream flow, and other parameters - to their values in upstream flow.

To complete the finite-differences system of the Navier-Stokes equations, following boundary conditions have been used. The no-slip conditions ($u = v = 0$), constant surface temperature ($T = T_w$), and extrapolations of a pressure from inner area nodes (with the condition $\partial p/\partial \eta = 0$) were posed on the body surface. On the outer surface of the computational area around the body, boundary conditions were written in the form of Riemann invariants and determined by the direction of perturbation expansion (see Ref. 8 for details).

The Approximation of Equations.

The construction of a finite-difference scheme to solve the Navier-Stokes equations (1) given in conservation laws form is based upon an integro-interpolation method.[8] The utilization of an integro-interpolation method applied to the solution of the Navier-Stokes equations gives finite-differences conservation laws analogies:

$$\frac{\mathbf{Q}_{j,k}^{n+1} - \mathbf{Q}_{j,k}^{n}}{\tau} + \frac{\mathbf{E}_{j+1/2,k}^{n+1} - \mathbf{E}_{j-1/2,k}^{n+1}}{h_\xi} + \frac{\mathbf{G}_{j,k+1/2}^{n+1} - \mathbf{G}_{j,k-1/2}^{n+1}}{h_\eta} = \mathbf{B}_{j,k}^{n+1} \qquad (7)$$

Here index n corresponds to time layer number; j, k - to node numbers along ξ and η, correspondingly; h_ξ, h_η - to the node sizes. The developed conservative finite-difference scheme is implicit, and this property of the scheme allows to avoid any restrictions on the iteration time-step caused by the instability of the ordinary difference schemes in the solution of the stiff differential equations.

At semi-integer nodes, the convective components of the flux vectors **E** and **G** were approximated using a monotonized scheme of the Godunov's type.[9] The eigenvalues and eigenvectors at semi-integer nodes were calculated by the Roe's method[10], for the approximate solution of the problem of arbitrary discontinuity decay:

$$\mathbf{E}_{j+1/2} = \frac{1}{2}(\mathbf{E}(\mathbf{Q}_L) + \mathbf{E}(\mathbf{Q}_R) - \mathbf{R}(\mathbf{Q}_{LR})\,\Phi(\Lambda_{LR})\,\mathbf{R}(\mathbf{Q}_{LR})^{-1}(\mathbf{Q}_R - \mathbf{Q}_L)) \qquad (8)$$

Here $\Phi(\Lambda_{LR})$ is a diagonal matrix with elements $\phi(\lambda_i)$; parameters λ_i are the eigenvalues of the operator $\mathbf{A} = \partial\mathbf{E}/\partial\mathbf{Q}$; and $\mathbf{R}_{LR} = \mathbf{R}(\mathbf{Q}_{LR})$ is a matrix with the columns being the right-hand side eigenvectors of the operator **A**. The function $\phi(\lambda)$ has the form:

$$\phi(\lambda) = \begin{cases} |\lambda|, & |\lambda| > \varepsilon \\ \dfrac{\lambda^2 + \varepsilon^2}{2\varepsilon}, & |\lambda| \le \varepsilon \end{cases} \qquad (9)$$

This form satisfies the "entropy" condition (or the criterion) in the choosing of a numerical solution with the correct physical properties.

To increase the order of finite-difference approximations up to the second one, the MUSCL-principle of the minimum derivatives[11] was used to interpolate dependent variables on the node side as follows:

$$\mathbf{Q}_L = \mathbf{Q}_j + \frac{1}{2}\,\mathrm{minmod}(\mathbf{Q}_j - \mathbf{Q}_{j-1}, \mathbf{Q}_{j+1} - \mathbf{Q}_j),$$
$$\mathbf{Q}_R = \mathbf{Q}_j - \frac{1}{2}\,\mathrm{minmod}(\mathbf{Q}_{j+1} - \mathbf{Q}_j, \mathbf{Q}_{j+2} - \mathbf{Q}_{j+1}) \qquad (10)$$

The function minmod(a,b) has the form:

$$\min\mathrm{mod}(a,b)=\begin{cases} a, & ab>0, \quad |a|<|b| \\ b, & ab>0, \quad |a|\geq|b| \\ 0, & ab\leq 0 \end{cases} \qquad (11)$$

The Roe's method[10] to solve approximately the Riemann's problem of arbitrary discontinuity decay was utilized to compute eigenvalues and eigenvectors of the **A**-operator. Parameters $\Phi(\Lambda_{LR})$, $\mathbf{R}_{LR}$, $\mathbf{R}_{LR}^{-1}$ were calculated by the values of dependent variables, such as:

$$u_{LR}=\frac{u_L\sqrt{\rho_L}+u_R\sqrt{\rho_R}}{\sqrt{\rho_L}+\sqrt{\rho_R}}$$

$$v_{LR}=\frac{v_L\sqrt{\rho_L}+v_R\sqrt{\rho_R}}{\sqrt{\rho_L}+\sqrt{\rho_R}} \qquad (12)$$

$$c_{LR}=\frac{c_L\sqrt{\rho_L}+c_R\sqrt{\rho_R}}{\sqrt{\rho_L}+\sqrt{\rho_R}}$$

Here the parameter c indicates the local speed of sound.

The diffusion components of the flux vectors **E** and **G** at the node side were approximated by the second order central difference scheme:

$$\frac{\partial \mathbf{U}}{\partial \xi_{j+1/2,k}}=\frac{\mathbf{U}_{j+1,k}-\mathbf{U}_{j,k}}{h_\xi}$$

$$\frac{\partial \mathbf{U}}{\partial \eta_{j+1/2,k}}=\frac{\mathbf{U}_{j+1,k+1}+\mathbf{U}_{j,k+1}-\mathbf{U}_{j+1,k-1}-\mathbf{U}_{j,k-1}}{4h_\eta} \qquad (13)$$

Here the parameter **U** is a vector of non-conservative dependent variables.

The difference scheme pattern used for the approximation of the complete Navier-Stokes equations consists of 13 nodes. It was found, that the developed implicit nonlinear finite-difference scheme is absolutely stable in the case of the linear problem.

In present study, the numerical algorithm developed for the internal flow modeling has been adopted to study external hypersonic viscous flows. The construction of the computational mesh was made by numerical solution of the Christoffel-Schwarz transformation problem.[12] The technique of the mesh adoptation in the boundary layers at high Reynolds numbers[13] has been used in this study.

Solution of Nonlinear Differences Equations.

The nonlinear system of grid equations ($\mathbf{F(X)} = 0$, where **X** is a vector of unknown discrete functions) was solved using the modified Newton's method:

$$\mathbf{X}^{[k+1]}=\mathbf{X}^{[k]}-\tau_{k+1}\mathbf{D}^{-1}\mathbf{F}(\mathbf{X}^{[k]}) \qquad (14)$$

Here $\mathbf{D}=\partial\mathbf{F}/\partial\mathbf{X}$ is the Jacobi matrix; k is the iteration number. In computations, the regularization parameter τ_k was calculated by formula:

$$\tau_{k+1}=\frac{(\Delta\mathbf{X}^{[k]}-\Delta\mathbf{X}^{[k-1]},\mathbf{X}^{[k]}-\mathbf{X}^{[k-1]})}{(\Delta\mathbf{X}^{[k]}-\Delta\mathbf{X}^{[k-1]})^2} \qquad (15)$$

where $\Delta\mathbf{X}^{[k]}$ is a vector of corrections. The iteration process is convergent with the second order of the convergence rate and $\tau_k \to 1$.

The iteration Jacobi matrix was found by employing the procedure of finite increments of the residual vector of the required grid functions. The approximation of the Navier-Stokes equations determinates the type of the Jacobi **D**-operator, namely, the rarefied structure of triangular matrices and the initial 7×7-dense matrix coincide.

The system of linear algebraic equations obtained in a nonlinearity iteration was solved by expanding the matrix into a product of two triangular matrices **L** and **U**, where **L** is the lower triangular matrix and **U** is the upper triangular matrix, and $\partial\mathbf{F}/\partial\mathbf{X} = \mathbf{L}^*\mathbf{U}$. This operation was preceded by the analysis of the sparsity structure of matrices **L** and **U**. In order to reduce the total number of the arithmetic operations and economize on RAM, the variables were numbered using the generalized method of nested dissection[14,15]. This technique was successfully used many times in computational experiments and proved its effectiveness and reliability.[8]

Numerical Results

The calculations were mainly performed on the 101×101 grid of the O-type. The size of the nodes was automatically reduced near the body surface and in the vicinity of the symmetry plane. The example of the finite-difference grid in physical space is presented in Fig. 1.

The convergence and accuracy of the numerical solutions were tested by carrying out a series of calculations of hypersonic viscous flow about a cylinder (at Reynolds number $Re_{\infty r} = 10^4$ and Mach number in upstream flow $M_\infty = 5$) on the grids of different size. The analysis of the results[6] showed that the numerical solution of the problem is convergent. Calculations were carried out at the Work Station RS6000/58H.

To improve the convergence rate of the iteration process, the new technique of formation of the Jacobi matrix was used. The method is based upon the usage of a truncated 3×3-dense matrix. The computing time of each variant was reduced by the factor of three and was estimated as approximately 20 min.

The flowfield around the circular cylinder of radius r and a plate of length $L = 2r$ was calculated for a Mach number $M_\infty = 5$ and for a Reynolds number $Re_{\infty r} = 10^4$ and 10^5. It was assumed that $\gamma = 1.4$, and the body surface is isothermal at $T_w/T_\infty = 2$. The four cases were studied: **a)** the cylinder alone without a plate; **b)** the distance between the leading edge of the plate and the rear point of the cylinder is $\Delta/r = 0$; **c)** $\Delta/r = 1$; **d)** $\Delta/r = 2$.

The contours of constant values of local Mach number M at $Re_{\infty r} = 10^4$ and temperature T/T_∞ at $Re_{\infty r} = 10^5$ are shown in Figs. 2 and 3, correspondingly, for all four cases considered. Under the testing conditions, the flowfield can be characterized by existing shock waves near the cylinder and in the wakes behind it, as well as by a wide separation area in the rear zone of the cylinder. The major differences of the flow patterns occur in this zone.

The distributions of flow parameters along the plane of symmetry in the wakes behind the cylinder at $Re_{\infty r} = 10^5$ are shown in Fig. 4. The geometrical factor of plate location, Δ/r, influences significantly the temperature and Mach number parameters. The pressure profiles are approximately the same in the cases considered.

The existence of the plate changes significantly the parameters of the flow near the rear part of the cylinder at $Re_{\infty r} = 10^5$ (see Fig. 5). The heat flux on the rear cylindrical surface is extremely sensitive to the plate location. At $\Delta/r = 2$, the heat flux increases by the factor of 10 in comparison with the case of flow around the cylinder without a plate. But at $\Delta/r = 0$, the value of the heat flux becomes its magnitude at the original level. This pattern of the parameter behavior is similar in the case of pressure distribution. The skin friction is at the same level in cases of separation between cylinder and plate. At $\Delta/r = 0$, its magnitude is negligible in the vicinity of the rear point of the cylinder.

The major effect of the plate location can be observed on the distributions of skin friction and heat flux along the plate surface (see Figs. 6 and 7). The skin friction is significantly less than predicted by the hypersonic-viscous-flow theory.[1-4] The heat flux distribution has extremum (maximum) near the leading edge of the plate in the specific case of the plate location at $\Delta/r = 2$. In this case the width of the recirculation zone behind the cylinder is comparable with the distance between the cylinder and the leading edge of the plate.

Summary

The flow parameters near a cylinder with no end contribution and a plate located in the wakes of a cylinder have been evaluated numerically for a wide range of geometrical parameters Δ/r. This parameter influences skin friction and heat flux distribution along the plate and cylinder surfaces. Also, it has been found that the plate location affects the temperature and velocity fields in the wakes behind the cylinder. Further numerical studies will be carried out to analyze the flow patterns in the strong interaction hypersonic regime.

References

[1]Hayes, W. D., and Probstein, R. F., *Hypersonic Flow Theory*, Academic Press, New York, NY, 1959.

[2]Oguchi, H., "The Sharp-Leading-Edge Problem in Hypersonic Flow," *Proceedings of the Second International Symposium on Rarefied Gas Dynamics*, Academic Press, New York, NY, 1961.

[3]Allegre, J., and C., Bisch, "Angle of Attack and Leading Edge Effects on the Flow about a Flat Plate at Mach Number 18," *AIAA Journal*, Vol. 6, No. 5, May 1968, pp. 848-852.

[4]Gusev, V. N., Erofeev, A. I., Klimova, T. V., Perepukhov, V. A., Riabov, V. V., and Tolstykh, A. I., "Theoretical and Experimental Investigations of Flow over Simple Shape Bodies by a Hypersonic Stream of Rarefied Gas," *Trudy TsAGI*, Issue 1855, 1977, pp. 3-43 (in Russian).

[5]Coudeville, H., Viviand, H., Raffin, M., and Brun, E. A., "An Experimental Study of Wakes of Cylinders at Mach 20 in Rarefied Gas Flow," *Proceedings of the Sixth International Symposium on Rarefied Gas Dynamics*, Academic Press, New York, NY, 1969.

[6]Bashkin, V. A., Egorov, I. V., and Egorova, M. V., "Supersonic Viscous Perfect Gas Flow Past a Circular Cylinder," *Fluid Dynamics*, No. 6, Nov.-Dec. 1993, pp. 833-838.

[7]Bisch, C., "Drag Reduction of a Sharp Flat Plate in a Rarefied Hypersonic Flow," *Proceedings of the Tenth International Symposium on Rarefied Gas Dynamics*, Vol. 1, AIAA, Washington, D.C., 1976, pp. 361-377.

[8]Yegorov, I., and Zaitsev, O., "Development of Efficient Algorithms for Computational Fluid Dynamic Problems," *Proceedings of the Fifth International Symposium on Computational Fluid Dynamics*, Sendai, 1993, Vol. III, pp. 393-400.

[9]Godunov, S. K., "Finite Difference Method for Numerical Computation of Discontinuous Solutions of the Equations of Fluid Dynamics," *Matematicheskii Sbornik*, Vol.47, 1959, pp. 271-306 (in Russian).

[10]Roe, P. L., "Approximate Riemann Solvers, Parameter Vectors, and Difference Scheme," *Journal of Computational Physics*, Vol. 43, 1981, pp. 357-372.

[11]Kolgan, V. P., "Application of the Principle of Minimum Value of Derivatives to the Construction of Finite-Difference Schemes for Calculating Discontinuous Solutions of Gas Dynamics," *Uchenye Zapiski TsAGI*, Vol. 3, No. 6, 1972, pp. 68-77 (in Russian).

[12]Yegorov, I. V., and Ivanov, D. V., "Application of the Complete Implicit Monotonized Finite-Differential Schemes in Modeling Internal Plane Flows," *Journal of Computational Mathematics and Mathematical Physics*, Vol. 36, No. 12, 1996, pp. 91-107.

[13]Bashkin, V. A., Yegorov, I. V., and Ivanov, D. V., "Application of Newton's Method to Calculation of Supersonic Internal Separation Flows," *Journal of Applied Mechanics and Technical Physics*, Vol.37, No.1, 1997.

[14]Lipton, R. J., Rose, D. J., and Tarjan, R. E., "Generalized Nested Dissection," *SIAM Journal of Numerical Analysis*, Vol. 16, 1979, pp. 346-351.

[15]Egorov, I. V., and Zaitsev, O. L., "On an Approach to the Numerical Solution of the Two-Dimensional Navier-Stokes Equations by the Shock Capturing Method," *Journal of Computational Mathematics and Mathematical Physics*, Vol. 31, No. 2, 1991, pp. 286-299.

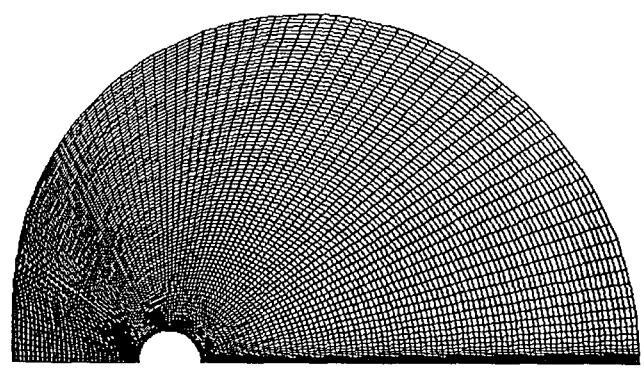

Fig. 1 Finite-difference grid in physical space.

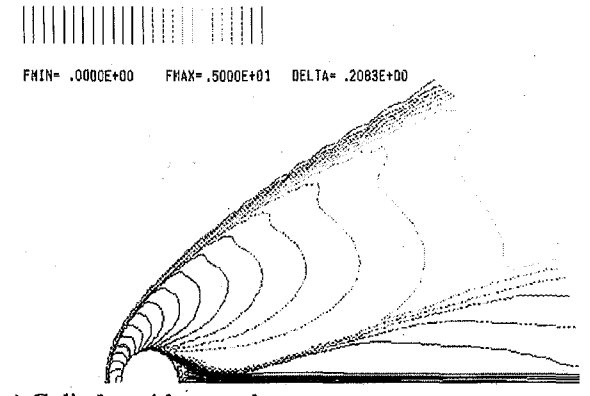

a) Cylinder without a plate

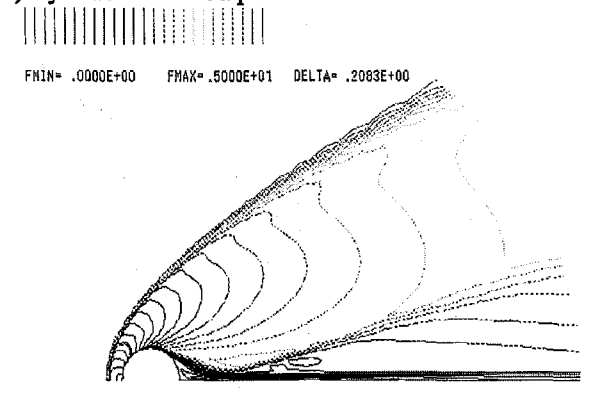

b) Cylinder and plate, Δ/r=0

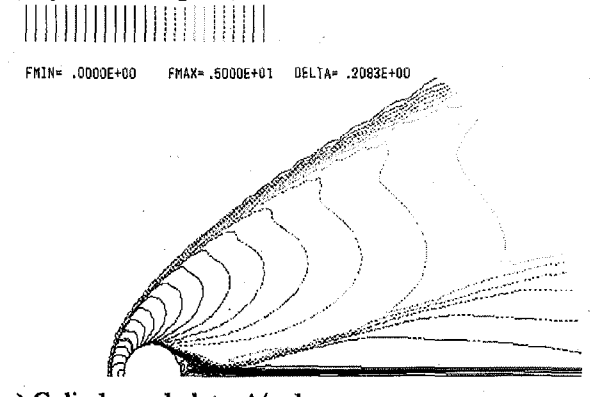

c) Cylinder and plate, Δ/r=1

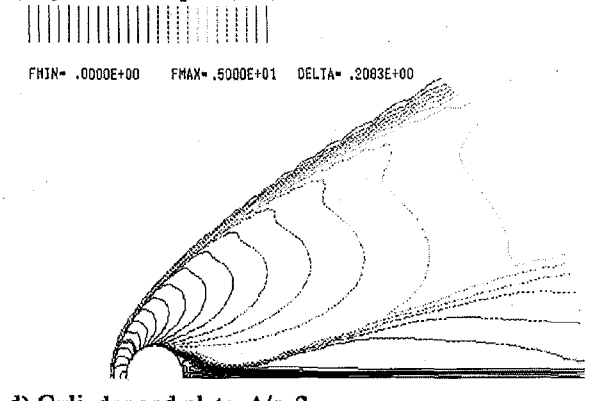

d) Cylinder and plate, Δ/r=2

Fig.2 Mach number contours at Re=10^4

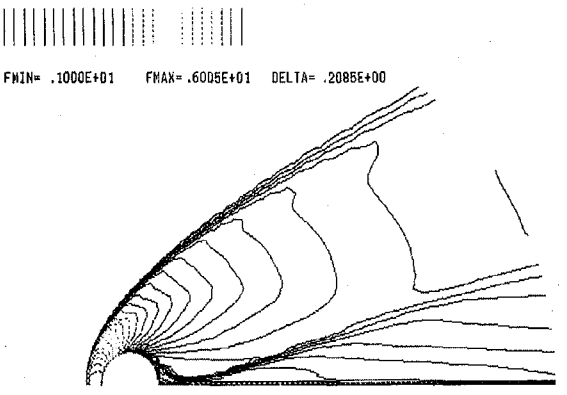

a) Cylinder without a plate

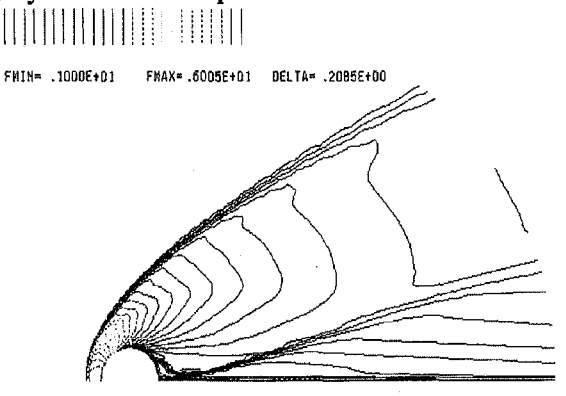

b) Cylinder and plate, Δ/r=0

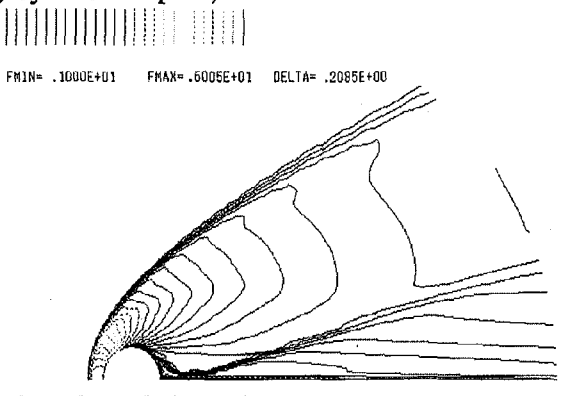

c) Cylinder and plate, Δ/r=1

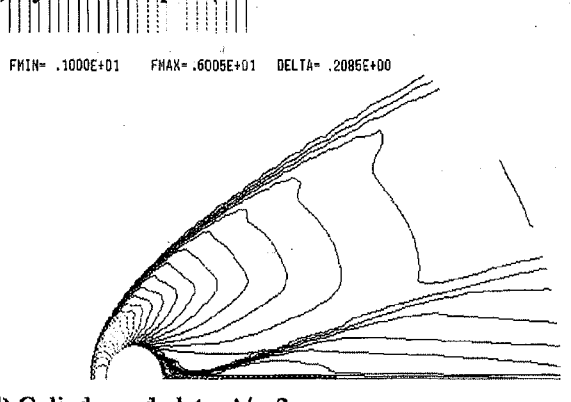

d) Cylinder and plate, Δ/r=2

Fig.3 Temperature contours at Re=10^5

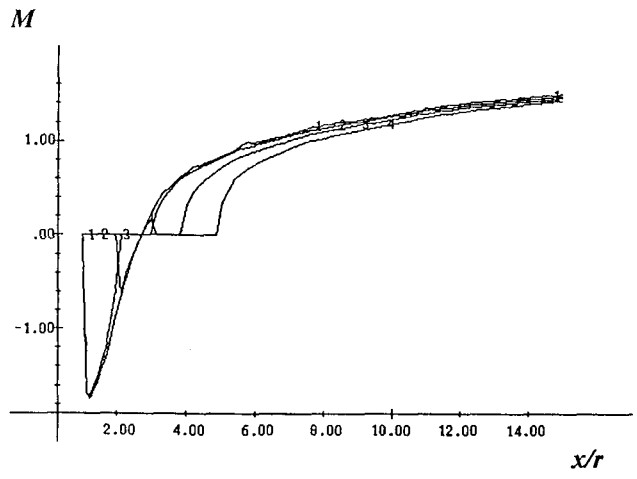

a)

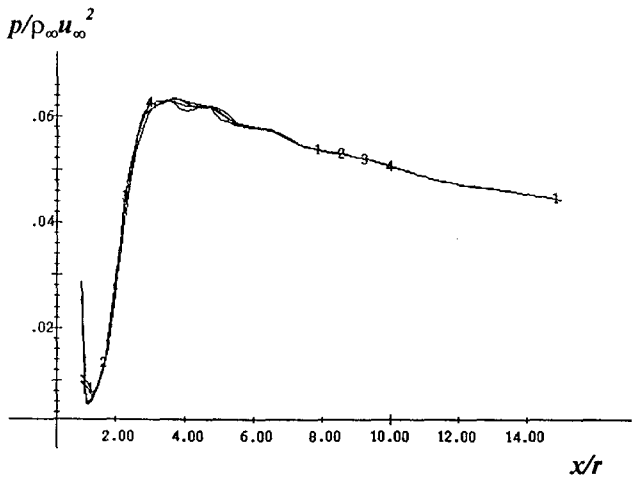

b)

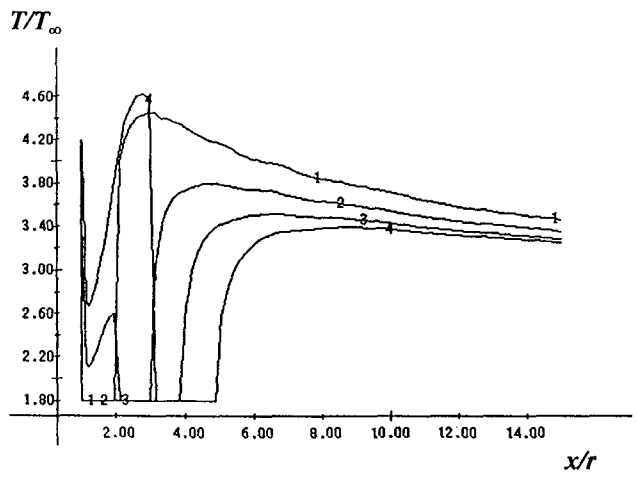

c)

Fig. 4 The flow parameters along the plane of symmetry in the wakes behind a cylinder at $M_\infty = 5$, $Re = 10^5$: a) Mach number, M; b) normalized pressure, $p/\rho_\infty u_\infty^2$; c) normalized temperature, T/T_∞. Curve 1 - cylinder without a plate; curve 2 - cylinder and plate, $\Delta/r = 0$; curve 3 - $\Delta/r = 1$; curve 4 - $\Delta/r = 2$.

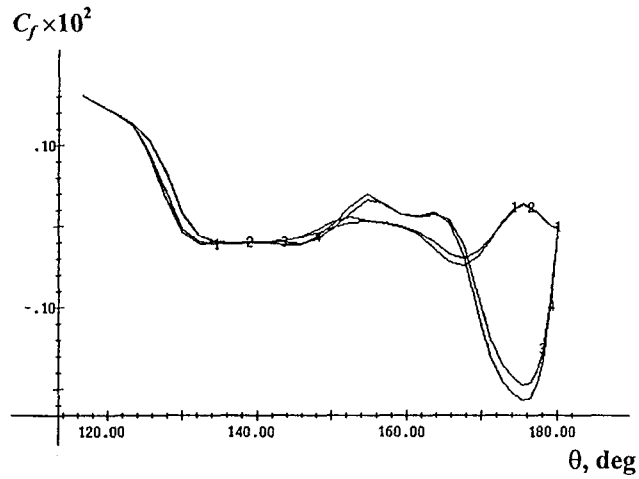

a)

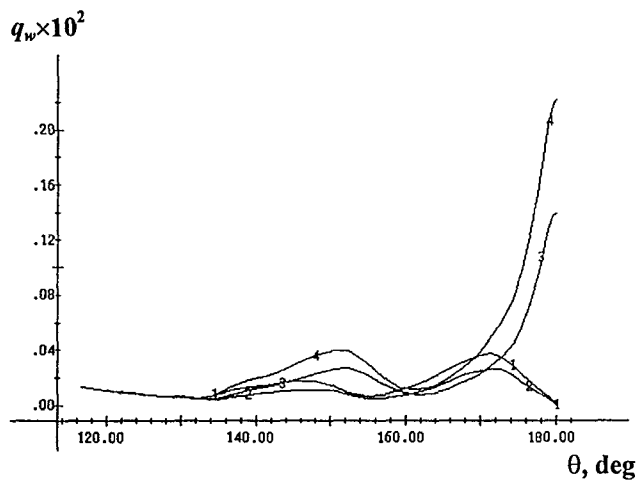

b)

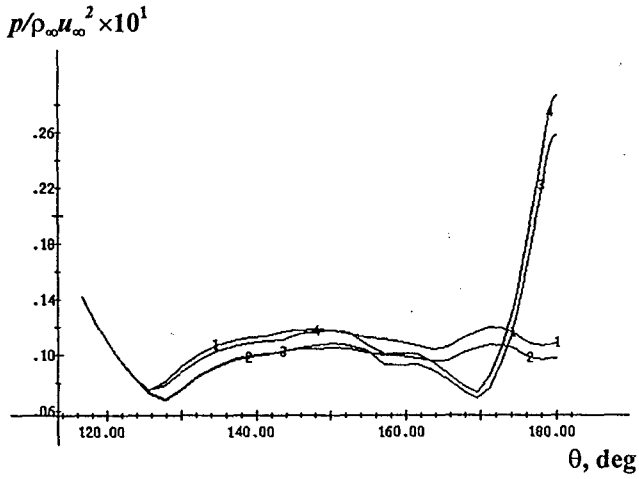

c)

Fig. 5 The distribution of flow parameters along the rear surface of a cylinder at $M_\infty = 5$, $Re = 10^5$: a) skin-friction coefficient, C_f; b) heat flux, q_w; c) normalized pressure, $p/\rho_\infty u_\infty^2$. Curve 1 - cylinder without a plate; curve 2 - cylinder and plate, $\Delta/r = 0$; curve 3 - $\Delta/r = 1$; curve 4 - $\Delta/r = 2$.

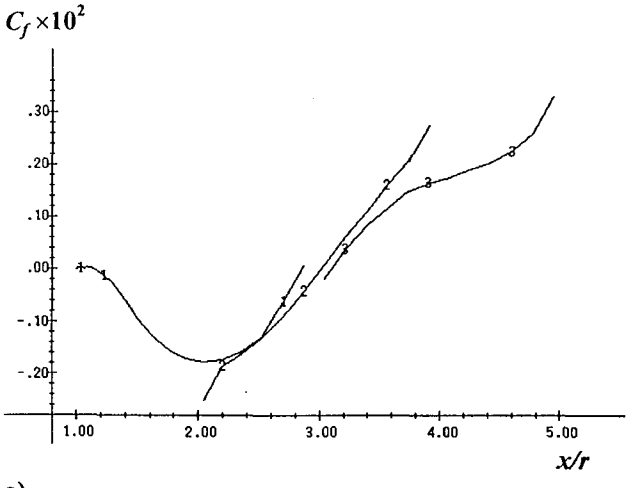

a)

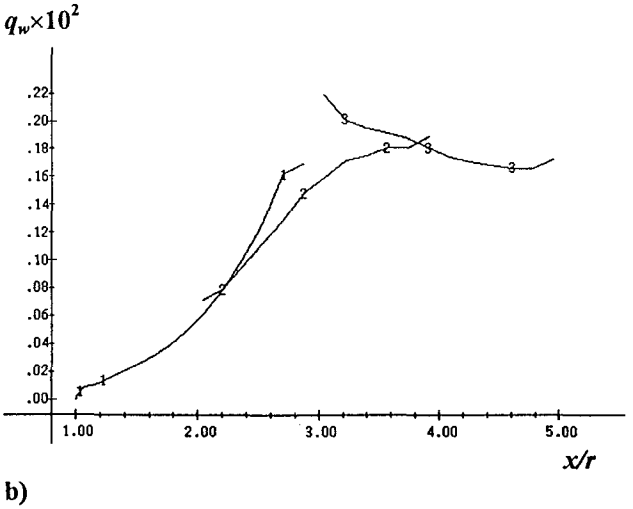

b)

Fig. 6 The distribution of flow parameters along the plate surface at $M_\infty = 5$, $Re = 10^4$: a) skin-friction coefficient, C_f; b) heat flux, q_w. Curve 1 - cylinder and plate, $\Delta/r = 0$; curve 2 - $\Delta/r = 1$; curve 3 - $\Delta/r = 2$.

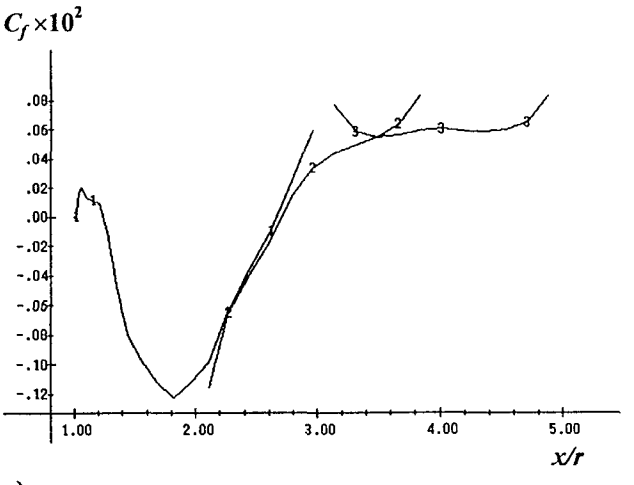

a)

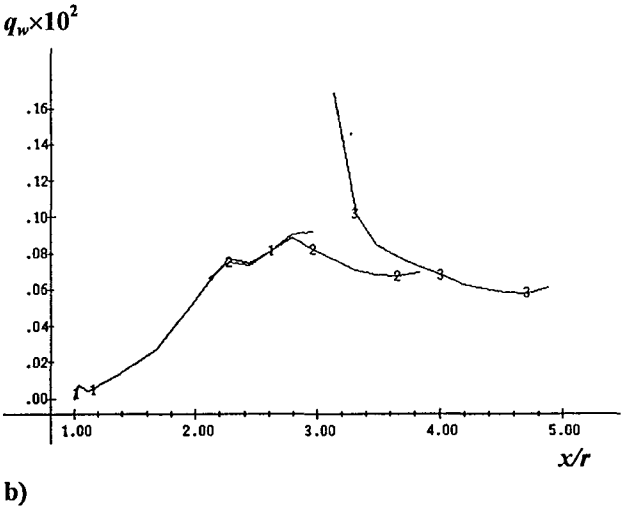

b)

Fig. 7 The distribution of flow parameters along the plate surface at $M_\infty = 5$, $Re = 10^5$: a) skin-friction coefficient, C_f; b) heat flux, q_w. Curve 1 - cylinder and plate, $\Delta/r = 0$; curve 2 - $\Delta/r = 1$; curve 3 - $\Delta/r = 2$.